Geophysical Journal International

Geophys. J. Int. (2017) **209,** 509–516
Advance Access publication 2017 January 25
GJI Gravity, geodesy and tides

doi: 10.1093/gji/ggx032

Excitation of the Earth's Chandler wobble by a turbulent oceanic double-gyre

S.E. Naghibi,[1,2] M.A. Jalali,[3,4] S.A. Karabasov[2] and M.-R. Alam[4]

[1] *Department of Mechanical Engineering, Sharif University of Technology, P.O. Box* 11155-9567, *Tehran, Iran*
[2] *School of Engineering and Materials Science, Queen Mary University of London, Mile End Rd, London E*1 4*NS, United Kingdom*
[3] *Department of Astronomy, University of California, Berkeley, CA* 94720, *USA. E-mail: mjalali@berkeley.edu*
[4] *Department of Mechanical Engineering, University of California, Berkeley, CA* 94720, *USA*

Accepted 2017 January 23. Received 2017 January 19; in original form 2016 July 22

SUMMARY

We develop a layer-averaged, multiple-scale spectral ocean model and show how an oceanic double-gyre can communicate with the Earth's Chandler wobble. The overall transfers of energy and angular momentum from the double-gyre to the Chandler wobble are used to calibrate the turbulence parameters of the layer-averaged model. Our model is tested against a multilayer quasi-geostrophic ocean model in turbulent regime, and base states used in parameter identification are obtained from mesoscale eddy resolving numerical simulations. The Chandler wobble excitation function obtained from the model predicts a small role of North Atlantic ocean region on the wobble dynamics as compared to all oceans, in agreement with the existing observations.

Key words: Earth rotation variations; Loading of the Earth; Atlantic Ocean; Fourier Analysis; Non-linear differential equations; Numerical modelling.

1 INTRODUCTION

Chandler wobble discovered in 1891 (Colombo & Shapiro 1968) is the turning of the Earth's rotation axis around the reference pole, and has an approximate period of 14 months determined by the rigidity and elliptic geometry of the Earth (Munk & MacDonald 1975). Being mainly damped by the internal friction in mantle and viscous dissipation in the outer fluid core (Smith & Dahlen 1981), Chandler wobble must decay to zero over decades. Its longevity for over a century therefore requires a continuous injection of energy and angular momentum from the oceans and atmosphere (Gross 2000; Gross *et al.* 2003; Adhikari & Ivins 2016), and powerful earthquakes (Dahlen 1971; Xu *et al.* 2014). Although a combination of geophysical processes is responsible for the excitation of the Chandler wobble, the exact role of the oceans and atmosphere is yet a matter of dispute. According to Brzezinski & Nastula (2002), the atmosphere and oceans provide 80 per cent of the excitation of Chandler wobble with approximately equal contributions. A comparison between non-atmospheric polar motion excitation function and oceanic angular momentum indicates that the transferred angular momentum of the external fluid layers composed of atmosphere, oceans and hydrology to the solid earth can fairly provide the total required energy for the observed Chandler wobble (Brzezinski *et al.* 2002, 2012). There are several studies, however, that do not favour equal contributions from the oceans and atmosphere, and find the atmosphere as the dominant source of Chandler wobble excitation (Furuya *et al.* 1996; Aoyama & Naito 2001), or even consider the oceans to have an attenuating role in the Earth's wobbling motion (Fang & Hager 2012).

Analytical modelling of the Chandler wobble was pioneered by (Smith & Dahlen 1981) and continued by Wahr (1982) who developed wobble excitation theory for a non-rigid Earth, including a fluid core and rotation-induced pole tides in the oceans (see also Wahr 1983). The natural frequencies of the coupled Earth–ocean system was then calculated (Wahr 1984; Dickman 1985), and it was shown that the long-period Markowitz wobble is a natural mode of the coupled mantle–ocean system (Dickman 1983). More recently, Nastula *et al.* (2012) have computed regional contributions of the oceans to the polar motion, and reported that the southern Indian ocean and south Pacific ocean have stronger effects on both the annual and Chandler wobble compared to Atlantic ocean. Regional multifluid-based excitation of the polar motion has also been investigated based on the geographic distribution of atmospheric pressure, the bottom pressure of the oceans, and land hydrology (Nastula *et al.* 2014). In later investigations, regional role of the oceans in the excitation of the polar motion is studied by computing correlations between the regional values of the oceanic excitation functions (obtained from ECCO/JPL data-assimilating model kf080) and global non-atmospheric excitations found through subtracting atmospheric angular momentum (AAM) series (NCEP/NCAR) from the time series of the polar motion provided by the International Earth Rotation and Reference Systems Service (IERS; Nastula *et al.* 2012, 2014). All these efforts centre on observational data and time-series analysis. For the first time, we intend to analytically investigate the

Table 1. Coefficients of effective angular momentum functions.

Model	α	β
Dickman's (2003) full coupling	$1.14155/(C-A)$	$1.60606/\Omega(C-A)$
Dickman's (2003) complete de-coupling	$1.09436/(C-A)$	$1.72402/\Omega(C-A)$

isolated effect of double-gyre dynamics on the Earth's Chandler wobble.

This study aims at identifying the sources of dynamical coupling between wind-driven oceanic gyres and the Earth's rigid-body dynamics. We are particularly interested to understand how the development of turbulent eddies in oceanic gyres affects the wobble signal. We simulate an isolated double-gyre as a toy model of North Atlantic circulations and deliberately control flow parameters and boundary conditions to study how they affect the Chandler wobble components. Our governing equations of oceanic flows are Navier–Stokes equations in spherical coordinates (e.g. Dijkstra 2006; Lewis & Langford 2008) but modified to include eddy viscosity. We separate the equations of motion for the fluid domain to two scales—a large scale solution simulating the flow throughout the whole domain and a small scale solution to represent the eastward jet—and solve them using a Galerkin spectral approximation (e.g. Il'In & Filatov 1988; Fengler 2005). Smagorinsky's (1963) approximation is used to model unresolved scales in the turbulent regime over a wide range of Reynolds numbers. We also test our theory using a wind-driven, three-layer, quasi-geostrophic model of the oceans that captures most features of realistic gyres, such as their eastward jet streams. Our idealized, efficiently computable, depth-averaged, double-gyre model predicts North Atlantic interactions with the Earth's Chandler wobble in the same way as the quasi-geostrophic double gyre model does in an eddy resolving regime. Our simulations of the North Atlantic predict approximately one-sixth of the observed contribution of global oceanic currents to the Chandler wobble excitation signal.

2 MODEL AND METHODS

We consider the rotating coordinate frame (x_1, x_2, x_3) attached to the Earth's centre, where x_3 is the axis corresponding to maximum rotary inertia and x_1 and x_2 are the other two principal axes within the equatorial plane. The unit base vector associated with the coordinate x_i is denoted by $\boldsymbol{e}_i$ $(i = 1, 2, 3)$. We define the total angular momentum of our system, composed of the Earth and oceans, by $\boldsymbol{H}$ and its absolute angular velocity by $\boldsymbol{\omega}$. The attitude dynamics of the system is thus described by Liouville's equation (see Munk & MacDonald 1975)

$$\frac{\mathrm{d}\boldsymbol{H}}{\mathrm{d}t} + \boldsymbol{\omega} \times \boldsymbol{H} = \boldsymbol{d}, \qquad \boldsymbol{H} = \mathbf{I} \cdot \boldsymbol{\omega} + \boldsymbol{h}. \tag{1}$$

Here $\boldsymbol{d}$ is the vector of external torques exerted by the solar system objects and atmospheric winds, and

$$\boldsymbol{h} = \int_V \rho\, \boldsymbol{r} \times \boldsymbol{v}\, \mathrm{d}V, \tag{2}$$

is the relative angular momentum vector of geophysical fluids (including the oceans and the Earth's outer core) with respect to the rotating Earth. The Earth is represented as a homogeneous non-rigid ellipsoid deformed due to centrifugal acceleration with or without taking into account the mantle-core interaction. In the angular momentum integral (eq. 2), ρ is the density of ocean water, $\mathrm{d}V$ is the infinitesimal volume of an ocean element with the position vector $\boldsymbol{r}$ and relative velocity $\boldsymbol{v}$. Wobble dynamics is described by perturbing the angular velocity $\boldsymbol{\omega}$ and the moment of inertia tensor $\mathbf{I}$ as

$$\boldsymbol{\omega} = \Omega \boldsymbol{e}_3 + \Omega\,(m_1 \boldsymbol{e}_1 + m_2 \boldsymbol{e}_2 + m_3 \boldsymbol{e}_3)\,, \tag{3}$$

$$\mathbf{I} = \mathbf{I}_0 + \boldsymbol{\Delta}\mathbf{I}, \qquad \mathbf{I}_0 = \mathrm{diag}\,[A, A, C]\,, \tag{4}$$

where Ω is the reference spin rate of the Earth, m_1 and m_2 are Chandler wobble components and m_3 is the variation rate of the length of the day. The matrix $\boldsymbol{\Delta}\mathbf{I}$ represents the variation of the moment of inertia tensor due to redistribution of mass. The constant parameter A is the Earth's moment of inertia around its principal axes in equatorial plane and C is its polar moment of inertia. The evolution of the Chandler wobble components is governed by (Munk & MacDonald 1975)

$$\frac{i}{(\sigma_0 + i/2Q)} \frac{\mathrm{d}\boldsymbol{m}}{\mathrm{d}t} + \boldsymbol{m} = \boldsymbol{\Psi} = \left[1 - \frac{i}{\Omega}\frac{\mathrm{d}}{\mathrm{d}t}\right]\{\alpha\, \boldsymbol{c} + \beta\, \boldsymbol{h}\}\,. \tag{5}$$

In this equation, we have $\boldsymbol{m} = m_1 + i m_2$, $\boldsymbol{\Psi} = \psi_1 + i\psi_2$, $\boldsymbol{h} = h_1 + i h_2$, $\boldsymbol{c} = c_{13} + i c_{23}$, σ_0 is the Chandler wobble frequency with the period $T_0 = 2\pi/\sigma_0 \approx 14$ months, and Q is the quality factor characterizing the oscillation bandwidth with respect to central Chandler frequency. The constants α and β depend on (i) the elastic response of the ocean–earth system to angular velocity perturbations and (ii) the assumptions on the Earth's core–mantle couplings. We consider the two cases of fully coupled and decoupled core–mantle system with corresponding values of α and β given in Table 1 adopted from table 1 in Dickman (2003), and investigate the sensitivity of the resulting polar motion components to core–mantle interaction when the polar motion is excited by an oceanic double-gyre. Notably, equation (5) is coupled to the velocity and acceleration fields of the oceans through $\boldsymbol{h}$ vector defined in eq. (2). In what follows, we first consider models of the Chandler wobble without the wobble's feedback on the ocean dynamics, then address the feedback effect.

We introduce an idealized double-gyre model described by single-layer Navier–Stokes equations solved in two scales and modified for turbulent viscosity effects. As a reference solution, we utilize a classical multilayer, quasi-geostrophic model of an oceanic double-gyre. Both models are applied to a closed basin within a longitude-latitude quadrangle. Our single and multilayer models are suitable for understanding subpolar and subtropical ocean gyres as well as nonlinear western boundary currents, such as the Gulf Stream or Kuroshio, and their eastward jet extensions.

The tidal effects of the oceans on the wobble dynamics are implicitly agglomerated in the definitions of α and β in eq. (5). In the scope of our ocean model, we are specifically interested in the effect of mesoscale turbulence on the Chandler wobble. We therefore utilize quasi-geostrophic approximation as the reference ocean model, which explicitly captures the mesoscale oceanic flows and averages out small-scale processes such as surface and internal gravity waves. In the framework of the quasi-geostrophic ocean model, there is no significant mass transfer between the vertical isopycnal layers; consequently, the coupling of the wobble dynamics to the ocean dynamics involves only the angular momentum term, $\boldsymbol{h}$, and

the term in eq. (5) that accounts for non-hydrostatic vertical mass transfer is ignored, $\boldsymbol{c} = 0$.

The reference quasi-geostrophic multi-layer model represents wind-driven double-gyre circulation in a mid-latitude basin confined to north-south and east–west solid walls. The model stratification is described by three isopycnal layers dynamically coupled through pressure variations. The governing equations consist of stratified three-layer, quasi-geostrophic potential vorticity equations (Holland 1978) with source terms coming from the meridional gradient of the Coriolis parameter, the lateral viscosity, bottom friction, and the wind forcing in Cartesian coordinates. We have

$$\partial_t q_i + J(\psi_i, q_i + \beta y) = \delta_{1i} F_w - \delta_{i3} \frac{a_v}{H_3^2} \Delta\psi_i + a_h \Delta^2 \psi_i, \quad i = 1, 2, 3, \tag{6}$$

where F_w, a_v and a_h are the wind curl forcing, bottom friction and lateral viscosity coefficients respectively, $J(f, g) = f_x g_y - f_y g_x$, δ_{ij} is the Kronecker symbol and β is the planetary vorticity gradient equal to $2 \times 10^{-11}\,\mathrm{m^{-1}\,s^{-1}}$. The function q_i is the layer-wise potential vorticity defined as

$$q_i = \Delta\psi_i - (1 - \delta_{i1}) S_{i1} (\psi_i - \psi_{i-1}) - (1 - \delta_{i3}) S_{i2} (\psi_i - \psi_{i+1}). \tag{7}$$

Here S_{i1} and S_{i2} are stratification parameters associated with the first and second Rossby deformation radii chosen as $Rd_1 = 40$ km and $Rd_2 = 23$ km, respectively. The three layers of our ocean model have the depths of $H_1 = 250$, $H_2 = 750$ and $H_3 = 3000$ m. The mean distance of the ocean from the Earth's centre is set to $r_\mathrm{m} = r_\mathrm{max} - (H_1 + H_2 + H_3)/2$ where $r_\mathrm{max} = 6374$ km.

This model includes a parameter $0 \le \alpha < \infty$ that can handle partial slip boundary conditions $\partial_{nn}\psi_i - \alpha^{-1}\partial_n \psi_i = 0$ with full-slip ($\alpha \to \infty$) and no-slip ($\alpha = 0$) conditions as their limiting cases. The unit vector $\boldsymbol{n}$ defines normal to boundaries. The governing boundary value problem (6) is solved using the high-resolution CABARET method (Karabasov *et al.* 2009; Shevchenko & Berloff 2015). All parameters of the reference quasi-geostrophic model have been specifically tailored for the North Atlantic region. Including other oceanic regions requires appropriate recalibration of the underlying quasi-geostrophic model to account for (i) relevant density stratification profile that depends on the local Rossby deformation radius, and (ii) wind forcing parametrization that depends on the local atmosphere–ocean interactions.

In our single-layer model, the streaming of an incompressible fluid element in the rotating frame (x_1, x_2, x_3), which rotates with the angular velocity $\boldsymbol{\omega}$, is governed by the continuity equation $\nabla \cdot \boldsymbol{v} = 0$ and the momentum equation:

$$\frac{\partial \boldsymbol{v}}{\partial t} + (\boldsymbol{v} \cdot \nabla)\boldsymbol{v} + 2\boldsymbol{\omega} \times \boldsymbol{v} + \dot{\boldsymbol{\omega}} \times \boldsymbol{r} + \boldsymbol{\omega} \times (\boldsymbol{\omega} \times \boldsymbol{r}) = \boldsymbol{f} - \frac{\nabla P}{\rho} + \frac{\nabla \cdot \boldsymbol{\tau}}{\rho} + \frac{\boldsymbol{T}}{h_w}, \tag{8}$$

where P is the hydrostatic pressure, $\boldsymbol{f}$ is the body force (per unit mass), $\boldsymbol{T}$ is the wind traction on ocean surface per unit density, $\boldsymbol{\tau}$ is deviatoric stress tensor and h_w is the ocean depth affected by wind forcing. The depth h_w is equivalent to H_1 in the three-layer quasi-geostrophic model. According to the definition of $\boldsymbol{\omega}$ in eq. (3), Navier–Stokes equations are coupled to the Chandler wobble components.

After averaging eq. (8) through the ocean depth $H = H_1 + H_2 + H_3$, we attempted to solve the resulting equation using a spectral expansion that satisfied full-slip boundary

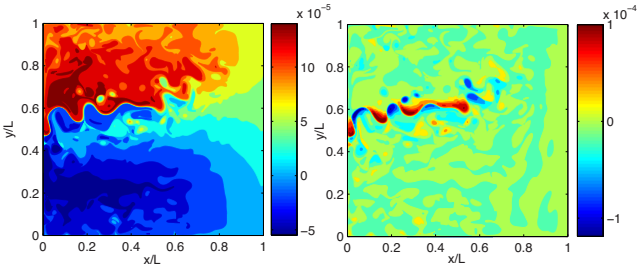

Figure 1. Top-layer instantaneous potential vorticity q_1 (left) and top-layer potential vorticity fluctuations q_1' (right) in a three-layer quasi-geostrophic double-gyre model. Contour lines indicate the magnitude of the function $q_1 = \Delta\psi_1 - S_{12}(\psi_1 - \psi_2)$ and its fluctuations. Left and right panels respectively demonstrate large- and small-scale vorticity evolution in both the time and space domains.

conditions. We started the solution procedure from zero initial conditions in presence of a steady sinusoidal wind stress. We found that constant horizontal and vertical viscosity coefficients (Dijkstra 2006) appearing in the expansion of diffusion terms $(\nabla \cdot \boldsymbol{\tau})$ in eq. (8) cannot stabilize the spectral solution in large-Reynolds-number regimes. We therefore adopted Smagorinsky's (1963) eddy viscosity approximation to obtain bounded solutions. We investigated the characteristics of the constructed spectral solutions and compared them with mesoscale features of North Atlantic ocean predicted by quasi-geostrophic double-gyre model. Our simulations showed that after implementing Smagorinsky's eddy viscosity, the single-layer spectral solution cannot capture an important characteristic of the double-gyre: its eastward jet. As Fig. 1 shows, the jet zone is associated with much smaller scales in space and time as well as large velocity amplitudes in comparison with the rest of the flow. The observation that a monolithic spectral solution is incapable of reproducing localized behaviours, with high-amplitude fast-evolving velocities, led us to develop a two-scale spectral solution for the depth-averaged double-gyre model.

In order to resolve the physics of jet streams in a double-gyre system, we base our two-scale solution on scale-decomposition modelling. We write

$$\boldsymbol{v} = \boldsymbol{v}^l + \boldsymbol{v}^L, \qquad \frac{l}{L} = \frac{\tau}{T} \ll 1, \qquad \frac{|\boldsymbol{v}^L|}{|\boldsymbol{v}^l|} \ll 1. \tag{9}$$

Here $\boldsymbol{v}^l$ and $\boldsymbol{v}^L$ are the small- and large-scale solutions of the velocity field, with l and L being the small and large length scales, respectively. The variables τ and T are the small and large time scales, respectively. The velocity field $\boldsymbol{v}^l$, which is introduced to describe jet characteristics, is nonzero over a narrow strip around the centreline of the two zonal lines $\theta = \theta_1'$ and $\theta = \theta_2'$ (with $\theta_1 < \theta_1', \theta_2' < \theta_2$), and $\boldsymbol{v}^L$ is nonzero everywhere in the domain. The jet position in the quasi-geostrophic model depends on the wind tilt, shift and asymmetry, and Reynolds number. We meridionally shift the centre of the small-scale zone to mimic the average position of the jet in the quasi-geostrophic model.

By substituting from eq. (9) into eq. (8) and making the resulting equation dimensionless, we split the Navier–Stokes equations into two coupled equations in two different scales where the coupling terms emerge due to the nonlinear convective terms $(\boldsymbol{v} \cdot \nabla)\boldsymbol{v}^l$ and $(\boldsymbol{v} \cdot \nabla)\boldsymbol{v}^L$. In small scales, since $|\boldsymbol{v}^L| \ll |\boldsymbol{v}^l|$, one can neglect the coupling of the small-scale momentum equation to large-scale

velocities. One can also approximate the small–scale velocity with its mean value. This yields

$$\overline{(\boldsymbol{v}^l \cdot \nabla)\boldsymbol{v}^l} - (\overline{\boldsymbol{v}}^l \cdot \nabla)\overline{\boldsymbol{v}}^l \approx 0, \tag{10}$$

where the bar sign denotes ensemble averaging. This approximation is valid up to the terms of $\mathcal{O}(l)$ and $\mathcal{O}(\tau)$. In other words, we assume that the small scales l and τ of the two-scale model represent the explicitly resolved small eddies of the reference many-scale eddy-resolving jet flow solution.

The coupling of large-scale momentum equation to small-scale velocities is not negligible. We assume that the unresolved part of the nonlinear Reynolds stress is equivalent to turbulence diffusion and write

$$\overline{(\boldsymbol{v} \cdot \nabla)\boldsymbol{v}^L} - (\overline{\boldsymbol{v}}^L \cdot \nabla)\overline{\boldsymbol{v}}^L = (\nabla.\overline{\tau}^L)^{\text{turbulence}}. \tag{11}$$

To compute $(\nabla \cdot \overline{\tau}^L)^{\text{turbulence}}$, we approximate the turbulent viscosity by Smagorinsky's (1963) vertical and horizontal eddy viscosity components:

$$\nu_v = (C_s\Delta)^2 \sqrt{2\left(2\bar{S}^L_{12}\bar{S}^L_{12} + 2\bar{S}^L_{13}\bar{S}^L_{13}\right)},$$

$$\nu_h = (C_s\Delta)^2 \sqrt{2\left(2\bar{S}^L_{22}\bar{S}^L_{22} + 2\bar{S}^L_{23}\bar{S}^L_{23} + S^L_{33}\bar{S}^L_{33}\right)}. \tag{12}$$

The coupling to small-scale velocities is thus compensated by turbulence. Here C_s is a constant parameter that parameterizes the turbulence, S^L_{ij} is the rate of deformation tensor in large scales with $\bar{S}^L_{ij}$ being its average over time. Denoting the cut off wave numbers in meridional and zonal spectral expansions by k_θ and k_ϕ, and the total ocean depth by H, the quantity $\Delta = [\pi^2 H/(k_\phi k_\theta)]^{1/3}$ will become the filter length-scale. Using the above assumptions, the governing equations of the small- and large-scale ocean dynamics become decoupled and can be solved separately. The final solution for the velocity field $\boldsymbol{v}$ can then be constructed by superposition.

We express eq. (8), which is now separated to decoupled equations in two scales, in terms of the spherical coordinates (r, θ, ϕ) where r is the radial distance from the centre of the Earth, and θ and ϕ are co-latitudinal and azimuthal angles, respectively. We confine our study to a quadrangle basin. Full slip boundary conditions are set along the zonal and meridional lines enclosing the large-scale solution domain $\mathcal{D}^L = \{(\theta, \phi)|\theta_1 \le \theta \le \theta_2, \phi_1 \le \phi \le \phi_2\}$ as well as the jet zone $\mathcal{D}^l = \{(\theta, \phi)|\theta'_1 \le \theta \le \theta'_2, \phi_1 \le \phi \le \phi_2\}$. We have

$$v^L_\theta\left(\theta_j, \phi, t\right) = v^L_\phi\left(\theta, \phi_j, t\right) = 0,$$

$$v^l_\theta\left(\theta'_j, \phi, t\right) = v^l_\phi\left(\theta, \phi_j, t\right) = 0, \quad j = 1, 2, \tag{13}$$

where $(v^l_r, v^l_\theta, v^l_\phi)$ and $(v^L_r, v^L_\theta, v^L_\phi)$ are respectively the components of $\boldsymbol{v}^l$ and $\boldsymbol{v}^L$ conjugate to (r, θ, ϕ) and we ignore the streaming of fluid elements in the radial direction and set $v^l_r = v^L_r = 0$. Since the small- and large-scale governing equations are completely decoupled as a result of scales separation and assumptions made in eqs (10) and (11), their boundary conditions will be imposed separately. In other words, $\boldsymbol{v}^L$ and $\boldsymbol{v}^l$ are governed by two distinct evolution equations in the two-scale model, and their linear superposition only approximately satisfies the original 'single-scale' eq. (8). We thus impose full-slip boundary conditions on both scales at their corresponding domain boundaries.

Taking the curl of the momentum equations eliminates the pressure P, centrifugal forces, and body forces (assuming they originate from conservative fields) from computations. Resulting equations are *vorticity transport* equations. The dominant component of the vorticity vector $\boldsymbol{\xi} = \nabla \times \boldsymbol{v}$ is in the r-direction (normal to the local horizon). We denote this normal component by $\xi_\perp = \frac{1}{\sin\theta}(\frac{\partial}{\partial\theta}(\sin\theta v_\phi) - \frac{\partial v_\theta}{\partial\phi})$ and solve its corresponding evolution equations presented below in both the small and large scales for (v^l_θ, v^L_θ) and (v^l_ϕ, v^L_ϕ) using a spectral Galerkin method:

$$\begin{aligned}
&\frac{\partial}{\partial t}\left(\frac{1}{\sin\theta}\left(\frac{\partial}{\partial\theta}\left(v^i_\phi \sin\theta\right) - \frac{\partial v^i_\theta}{\partial\phi}\right)\right) = 2\Omega v^i_\theta \sin\theta \\
&+ \frac{1}{r\sin\theta}\left(\frac{\partial v^i_\theta}{\partial\phi}\frac{\partial v^i_\theta}{\partial\theta} + v^i_\theta\frac{\partial^2 v^i_\theta}{\partial\theta\partial\phi} + \frac{1}{\sin\theta}\frac{\partial v^i_\phi}{\partial\phi}\frac{\partial v^i_\theta}{\partial\phi}\right. \\
&+ \frac{v^i_\phi}{\sin\theta}\frac{\partial^2 v^i_\theta}{\partial\phi^2} - v^i_\phi\frac{\partial^2 v^i_\phi}{\partial\theta\partial\phi} - 2v^i_\phi\cot\theta\frac{\partial v^i_\phi}{\partial\phi} - \sin\theta\frac{\partial v^i_\theta}{\partial\theta}\frac{\partial v^i_\phi}{\partial\theta} \\
&- v^i_\theta\sin\theta\frac{\partial^2 v^i_\phi}{\partial\theta^2} - v^i_\phi\cos\theta\frac{\partial v^i_\theta}{\partial\theta} + v^i_\phi v^i_\theta\sin\theta - \frac{\partial v^i_\phi}{\partial\theta}\frac{\partial v^i_\phi}{\partial\phi} \\
&\left.- 2v^i_\theta\cos\theta\frac{\partial v^i_\phi}{\partial\theta}\right) \\
&+ \frac{\left(a_h + \nu^i_h\right)}{r^2\sin\theta}\left[-\frac{\partial^2}{\partial\phi\partial\theta}\left(\frac{1}{\sin\theta}\frac{\partial}{\partial\theta}\left(v^i_\theta\sin\theta\right)\right)\right. \\
&+ \sin\theta\frac{\partial^2}{\partial\theta^2}\left(\frac{1}{\sin\theta}\frac{\partial}{\partial\theta}\left(v^i_\phi\sin\theta\right)\right) + 2\cot\theta\frac{\partial^2 v^i_\theta}{\partial\theta\partial\phi} \\
&+ \cos\theta\frac{\partial}{\partial\theta}\left(\frac{1}{\sin\theta}\frac{\partial}{\partial\theta}\left(v^i_\phi\sin\theta\right)\right) + \frac{\cot\theta}{\sin\theta}\frac{\partial^2 v^i_\phi}{\partial\phi^2} \\
&\left.+ \frac{1}{\sin\theta}\frac{\partial^3 v^i_\phi}{\partial\theta\partial\phi^2} - \frac{2}{\sin^2\theta}\frac{\partial v^i_\theta}{\partial\phi} - \frac{1}{\sin^2\theta}\frac{\partial^3 v^i_\theta}{\partial\phi^3}\right] \\
&+ \frac{\left(a_v + \nu^i_v\right)}{r^2\sin\theta}\frac{\partial}{\partial r}\left[r^2\frac{\partial}{\partial r}\left(\frac{\partial}{\partial\theta}\left(v^i_\phi\sin\theta\right) - \frac{\partial v^i_\theta}{\partial\phi}\right)\right] \\
&+ \frac{\tau^i_0}{H_1}\left[\frac{1}{\sin\theta}\left(\frac{\partial}{\partial\theta}\left(\tau_\phi\sin\theta\right) - \frac{\partial\tau_\theta}{\partial\phi}\right)\right] \\
&- 2r\Omega\left(\dot{m}_1\cos\phi + \dot{m}_2\sin\phi\right)\sin\theta.
\end{aligned} \tag{14}$$

Here $i \in \{l, L\}$ with l and L respectively denoting small and large scales, $\boldsymbol{T} = \tau_0(\tau_\theta, \tau_\phi)$ is the wind traction in eq. (8), and $v^l_h = v^l_v = 0$ according to eq. (10). The last term in eq. (14) represents the coupling of ocean dynamics to Chandler wobble components. Let us define $\Delta_\theta = (\theta_2 - \theta_1)/(2\pi)$, $\Delta_\phi = (\phi_2 - \phi_1)/\pi$ and $\Delta'_\theta = (\theta'_2 - \theta'_1)/(2\pi)$. Our spectral expansions have the form

$$v^L_\theta = \sum_{m,n} Y^L_{mn}(t)\sin(m w_\theta)\cos[(2n-1)w_\phi], \tag{15}$$

$$v^l_\theta = g(\theta'_1, \theta'_2)\sum_{m',n'} Y^l_{m'n'}(t)\sin(m' w'_\theta)\cos[(2n'-1)w_\phi], \tag{16}$$

$$\begin{aligned}
v^L_\phi = &-\sum_{m,n}\frac{\Delta_\phi Y^L_{mn}(t)}{(2n-1)}\sin[(2n-1)w_\phi] \\
&\times\left[\cos\theta\sin(m w_\theta) + \Delta^{-1}_\theta m\,\sin\theta\cos(m w_\theta)\right],
\end{aligned} \tag{17}$$

$$\begin{aligned}
v^l_\phi = &\, g(\theta'_1, \theta'_2)\sum_{m',n'}\frac{\Delta_\phi Y^l_{m'n'}(t)}{(2n'-1)}\sin[(2n'-1)w_\phi] \\
&\times\left[\cos\theta\sin(m' w'_\theta) + \Delta'^{-1}_\theta m'\,\sin\theta\cos(m' w'_\theta)\right],
\end{aligned} \tag{18}$$

where $w_\theta = (\theta - \theta_1)/\Delta_\theta$, $w_\phi = (\phi - \phi_1)/\Delta_\phi$, $w'_\theta = (\theta - \theta'_1)/\Delta'_\theta$, $g(\theta'_1, \theta'_2) = (H(\theta'_1) - H(\theta'_2))$, and $H(\theta'_1)$ and $H(\theta'_2)$ are Heaviside unit step functions. These spectral expansions satisfy

the boundary conditions (13) and the continuity equation. For the Reynolds number $Re = ULa_h^{-1}$ (where $L = 3840$ Km and $U = \tau_0(\rho_1 H_1 L\beta)^{-1} = 0.0417$) in the range $800 < Re < 8000$, the Coriolis and wind forcing terms are the dominant terms of the vorticity equations. Terms corresponding to convective acceleration, bottom friction and lateral (in-plane) viscosity are, respectively, the next important terms. Acceleration and terms corresponding to the Chandler wobble have the smallest orders of magnitude. We substitute the spectral expansions of (v_θ^l, v_θ^L) and (v_ϕ^l, v_ϕ^L) into the evolution equations of $\xi_\perp^l$ and $\xi_\perp^L$ (eq. 14), multiply the resulting equations by the following weight functions

$$\psi_{mn}^L = \frac{\sin(nw_\phi)\Delta_\phi}{n\sin\theta}\left[\frac{n^2\sin(mw_\theta)}{\Delta_\phi^2} - \cos^2\theta\sin(mw_\theta) + \left(1+\frac{m^2}{\Delta_\theta^2}\right)\sin(mw_\theta)\sin^2\theta - \frac{3m\cos(mw_\theta)\sin 2\theta}{2\Delta_\theta}\right], \tag{19}$$

$$\psi_{m'n'}^l = g(\theta_1', \theta_2')\frac{\sin(n'w_\phi)\Delta_\phi}{n'\sin\theta}\left[\frac{n'^2\sin(m'w_\theta')}{\Delta_\phi^2} - \cos^2\theta\sin(m'w_\theta') + \left(1+\frac{m'^2}{\Delta_\theta'^2}\right)\sin(m'w_\theta')\sin^2\theta - \frac{3m'\cos(m'w_\theta')\sin 2\theta}{2\Delta_\theta'}\right], \tag{20}$$

which have been obtained from eqs (15)–(18) and are associated with the normal component of the vorticity function $\xi_\perp = \frac{1}{\sin\theta}\left(\frac{\partial}{\partial\theta}(\sin\theta v_\phi) - \frac{\partial v_\theta}{\partial\phi}\right)$ in each scale. We then integrate over a discrete grid in the (θ, ϕ)-domain. This leads to a system of nonlinear ordinary differential equations $\dot{\boldsymbol{z}} = \boldsymbol{F}(\boldsymbol{z}, t)$ for the unknown amplitude functions $Y_{mn}^L(t)$ and $Y_{m'n'}^l(t)$, which have been collected in the time-dependent vector $\boldsymbol{z}(t)$. The Nonlinear ordinary differential equations $\dot{\boldsymbol{z}} = \boldsymbol{F}(\boldsymbol{z}, t)$ are solved using an adaptive fourth-order Runge–Kutta method with the relative accuracy of 10^{-4}. The maximum integration time step is 1 d.

3 RESULTS

In the single-layer spectral ocean model, the longitude-latitude quadrangle is defined by $\phi_1 = -\phi_2 = -0.4102$, $\theta_1 = \pi/6$ and $\theta_2 = 1.126$ radians, which correspond to a basin of the size 3840 km × 3840 km in the quasi-geostrophic ocean model. Our model double-gyre simulates the North Atlantic subpolar and subtropical gyres approximately located between the latitudes of Greenland and Canary Islands. We use the following steady parametrization model for the normal component of the curl of the wind field over the entire quadrangle domain

$$F_w = \begin{cases} A\sin\left(\frac{\pi(\pi/2-\theta)/(\theta_2-\theta_1)}{(\pi/2-\theta_0)/(\theta_2-\theta_1)}\right), & \frac{\pi}{2}-\theta_0 < \theta < \theta_2, \\ -B\sin\left(\frac{\pi(\theta_0-\theta)/(\theta_2-\theta_1)}{1-(\pi/2-\theta_0)/(\theta_2-\theta_1)}\right), & \theta_1 < \theta < \frac{\pi}{2}-\theta_0, \end{cases}$$

$$A = -\frac{2\pi\tau_0 \times W_{\text{asym}}}{H_1}, \quad B = \frac{2\pi\tau_0}{W_{\text{asym}} \times H_1},$$

$$\frac{\pi/2-\theta_0}{\theta_2-\theta_1} = 0.5 + W_{\text{tilt}}\left(\frac{\phi-\phi_1}{\phi_2-\phi_1} - 0.5\right), \tag{21}$$

where $\tau_0 = 0.8 \times 10^{-4}$ m^2 s^2, $W_{\text{asym}} = 0.9$ and $W_{\text{tilt}} = 0.2$ are the wind stress per unit density, wind asymmetry and tilt parameters, respectively (see Karabasov *et al.* 2009; Shevchenko & Berloff 2015). These parameters have been obtained by qualitatively mimicking the observational data of ocean dynamics in the reference quasi-geostrophic solution. Since the wind is assumed to be tilted and the jet dissipates as it moves eastwards, the average position of the jet peak is shifted to right in the quasi-geostrophic model. We have deliberately shifted the jet box of the small-scale solution in the spectral model so that the jet peaks of the two models coincide.

The quasi-geostrophic double-gyre model utilizes a numerical code based on CABARET (Karabasov & Goloviznin 2009) space–time scheme simulated here on 256 × 256 and 512 × 512 grids. The single-layer double-gyre model is solved using a two-scale spectral expansion involving nine terms in each scale ($M = 3, N = 3, M' = 3, N' = 3$), which cover two regions with different characteristics as described in Fig. 1. The bottom friction in both models is set to $a_v = 0.36$ m^2 s^{-1}, and for the linear horizontal viscosity a_h we have used 100 m^2 s^{-1}. Our computations for the single-layer model show that for large Reynolds numbers the application of constant horizontal and vertical viscosity components destabilizes spectral solutions. It was only after implementing Smagorinsky's eddy viscosity that we were able to find bounded spectral solutions for the streaming velocity.

We use the results of the spectral and numerical double-gyre models to compute the amount of angular momentum and kinetic energy that the double-gyre transfers to the Earth's Chandler wobble. We have post-processed the quasi-geostrophic outputs to calculate nodal velocities over a discrete grid in the zonal and meridional directions. The average angular momentum **h** and kinetic energy of the double-gyre are then computed over ≈10 yr period using both models: after 8000 d of spin-up time for the CABARET solution to become statistically stationary, and 10 000 d for the spectral code to become steady. In comparison with the single-scale spectral models considered, the current two-scale model not only includes the Smagorinsky eddy viscosity parameter but also the new parameter corresponding to the width of the small-scale zone, $r_m(\theta_2' - \theta_1')$ with respect to the computational box size $r_m(\theta_2 - \theta_1)$. Using these two parameters, the two-scale model is calibrated so that it preserves both the integral angular momentum and the integral kinetic energy of the reference eddy-resolved double-gyre solution. Fig. 2 shows the operating points in the parameter space corresponding to the two-scale model and the single-scale Smagorinksy model. The integral angular momentum and kinetic energy parameters are normalized on the values of the reference eddy-resolving solution of the double-gyre problem. To obtain the reference integral values, the corresponding unsteady eddy-resolving solution of the three-layer double-gyre problem was volume and time averaged. For the characteristic width of the jet flow region $\frac{\theta_2'-\theta_1'}{\theta_2-\theta_1} = 0.354$, which has the order of the lateral size of the meandering jet region in Fig. 1, and the value of Smagorinsky parameter C_s set to 0.1, the integral parameters of the two-scale model exactly match those of the reference double-gyre solution. In contrast to this, the single-scale Smagorinsky model cannot be calibrated to achieve the same: regardless of the viscosity parameters used, its kinetic energy is too damped or its angular momentum is excessively high as compared to the reference eddy-resolving simulation.

For further validation of the semi-analytical model developed, comparing its local flow solution features, such as the meanflow jet velocity profile, with the eddy-resolving solution is important. The two-scale model approximates the meandering jet with a parallel jet flow in the longitudinal direction so it cannot predict the evolving jet features. However, it can capture the main latitudinal jet profile as illustrated in Fig. 3 which compares the model prediction of the zonal velocity profile v_ϕ, with those of the time-averaged reference solution averaged over the half of the domain in the zonal direction $[\phi_1, (\phi_1 + \phi_2)/2]$. The latter averaging method is selected

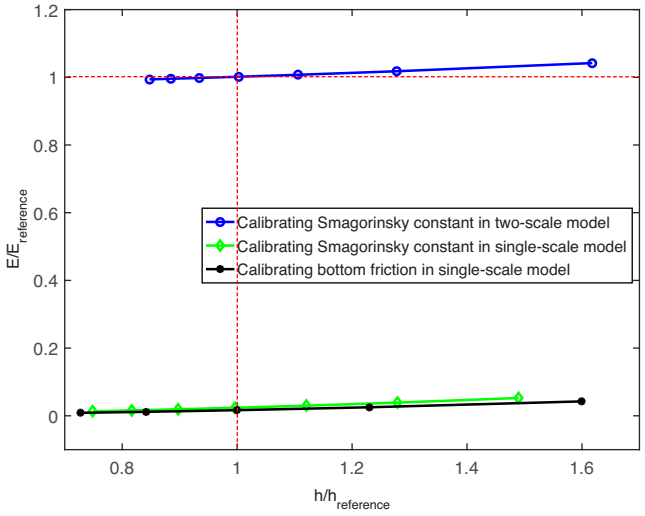

Figure 2. Different parametrizations used in the layer-averaged double-gyre model to capture the reference angular momentum and kinetic energy. The quantities $h_{\text{reference}}$ and $E_{\text{reference}}$ are computed using the numerical quasi-geostrophic ocean model. In a single-scale solution, which is incapable of predicting the right amount of kinetic energy, either of Smagorinsky's constant or the bottom friction coefficient can tune the overall angular momentum (diamond and star symbols). We have introduced Smagorinsky's constant as the control parameter because of its compatibility with the physics of turbulence. It is seen that two-scale solutions can capture the correct values of the kinetic energy and angular momentum of the double-gyre (circles).

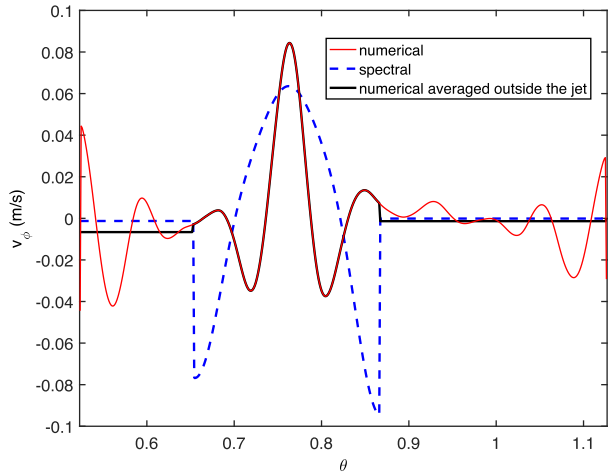

Figure 3. Time-averaged zonal velocity profile (v_ϕ) in the meridional direction (θ) representing the jet stream. The numerical solutions are calculated over a 512 × 512 grid and compared with the spectral two-scale solution, assuming an offset in the position of the jet box. Each velocity profile is obtained by average over all meridional sections along the jet, between the longitudes of $\phi = \phi_1$ and $\phi = \phi_1 + (\phi_2 - \phi_1)/2$.

so that the jet extension is completely included in the averaging domain of the eddy-resolving solution in accordance with Fig. 1. The latitude profile of the two-scale solution is compared with the reference eddy-resolving solution of the double-gyre problem that is layer and time averaged. In addition to the zonally averaged reference solution, the reference solution which is both zonally and latitude-wise averaged is shown on the same plot for comparison. It can be seen that the main jet profile is generally well captured by the simplified two-scale model. The model even predicts the two recirculation zones above and below the jet which are in a good qualitative agreement with the reference eddy-resolving solution.

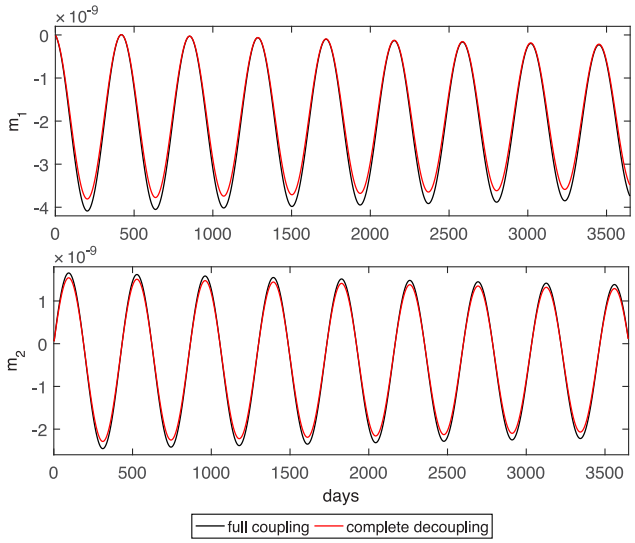

Figure 4. Comparison of Chandler wobble components fed by spectral solutions of the idealized double-gyre model in two cases of full core–mantle coupling and complete core–mantle decoupling

Further features of the double-gyre flow outside the jet region such as details of the boundary layer and recirculation flows close to the top and the bottom wall boundaries of the double gyre domain are not included in the semi-analytical two-scale model. Despite this, notably, the two-scale model correctly predicts the zonally and latitude-wise averaged state of the reference eddy resolving solution outside of the jet region.

Using spectral solutions of the idealized double-gyre model, we have compared the Chandler wobble components in two cases: fully coupled and decoupled core–mantle interactions (Fig. 4). Minor differences are distinguishable between the two models in their resulting polar motion components within the frame work of the toy model we have used for the ocean–Earth interactions. To conduct more accurate comparisons between the cases under study, we compute the excitation functions ψ_1 and ψ_2 (Chao 1985). In Fig. 5, we have shown the excitation functions computed from numerical CABARET solutions of the quasi-geostrophic double-gyre model on two different grids of 256 × 256 and 512 × 512 in the frequency domain. This helps us understand the numerical grid sensitivity of the model based on the eddy-resolved ocean dynamics simulation. We have also used spectral double-gyre solutions and numerical solutions over 256 × 256 and 512 × 512 grids to calculate the time-averaged norm $\sqrt{\psi_1^2 + \psi_2^2}$ of the excitation function for both the coupled and decoupled core–mantle interactions (Table 2).

Fig. 6 displays the time-series of the Chandler wobble components corresponding to the velocity fields of two double-gyre models, layer-averaged spectral and numerical quasi-geostrophic models. The time averaged kinetic energy and angular momentum of the numerical CABARET solutions over a 512 × 512 grid are used as the reference for calibration purposes, and numerical solutions depicted in Fig. 6 are computed over a 512 × 512 grid. All solutions shown in Fig. 6 are associated with a completely decoupled core–mantle model of an elastic Earth (Wahr 1982, 1983; Dickman 1993, 2003). We performed our spectral simulation with and without the influence of the Earth's wobbling motion on the double-gyre and Navier–Stokes equations. As Fig. 6 shows, the wobble excitation function does not change by including the wobble's feedback on the ocean dynamics.

Our findings suggest that the effect of the wobble on the North-Atlantic ocean dynamics is so small that it can be ignored in

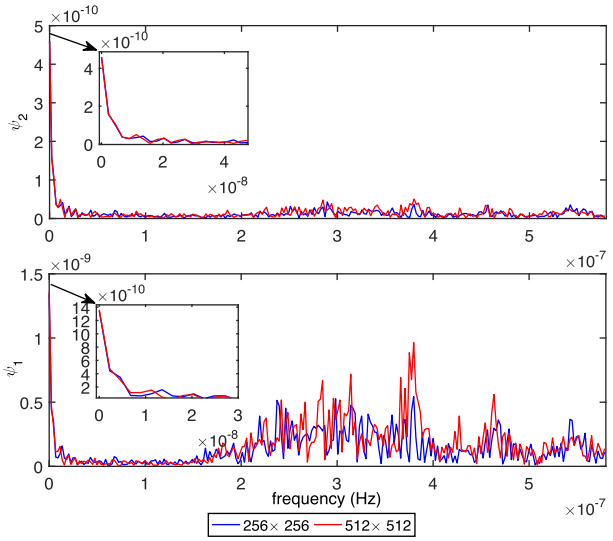

Figure 5. Comparison of Chandler wobble excitation function components calculated for numerical solutions of quasi-geostrophic model on 256 × 256 and 512 × 512 grids in case of complete core–mantle decoupling.

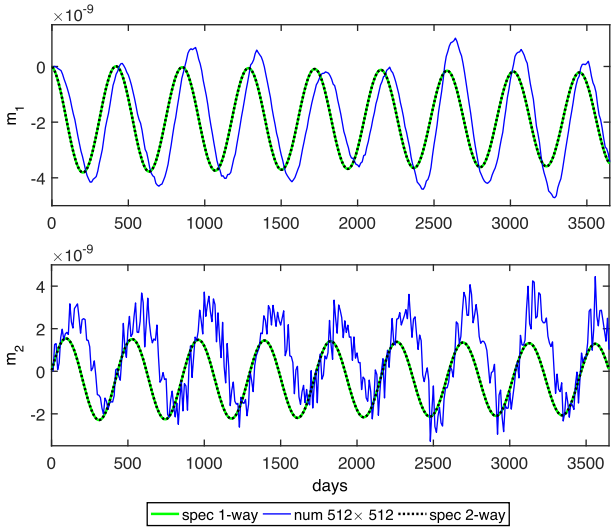

Figure 6. Comparison of Chandler wobble components fed by spectral and numerical double-gyre solutions belonging to the layer-averaged and quasi-geostrophic models respectively in case of complete core–mantle decoupling. Spectral solutions are plotted in case of 1-way and 2-way couplings and numerical solutions are calculated on 512 × 512 grid. The spectral solutions are virtually the same in 1-way and 2-way couplings.

comparison with the ocean–atmosphere interactions (wind forcing effect). To examine this hypothesis, we have conducted a series of additional simulations using our spectral model, with and without the feedback of the wobble to the oceans. These calculations have shown that no increase (e.g. 10–100 times fold) of the wind forcing amplitude leads to any appreciable difference between the 'one-way' and the 'two-way-coupled' wobble excitation functions. The difference in the two functions becomes notable only when one reduces the wind forcing by several orders of magnitude, hence making the wobbling effect comparable to other pertinent ocean dynamics processes. These results further suggest that there is no strong interaction between the ocean dynamics and the wobble for the ocean region studied. This conclusion is in a broad agreement with the analysis of Nastula *et al.* (2012, 2014) and Ma *et al.* (2009), who find that the effect of the North Atlantic region on the Earth's wobble is small as compared to the Pacific or Indian oceans.

Having justified the neglect of the feedback effect (from the wobble to the ocean dynamics), angular momentum components, computed using the one-way coupled numerical and spectral methods, are used to calculate the complex-valued Chandler wobble excitation function $\mathbf{\Psi} = \psi_1 + i\psi_2$. We have compared the average amplitude of simulated $\mathbf{\Psi}$ with the observed polar motion excitation spectral density originating from oceanic currents around the Chandler frequency. The amplitudes that we find (using both models) are around 0.4 mas, which is about an order of magnitude less as compared to the observed values corresponding to the global oceanic currents effect on the Chandler wobble excluding seasonal oscillations (approximately 2.4 mas) (Gross 2000; Nastula *et al.* 2012). Furthermore, the analysis of the oceans' velocity field from 1980 to 2005 using ECCO (Estimating the Circulation and Climate of the Ocean) marine circulation (Ma *et al.* 2009) show that among the three main oceans, Atlantic ocean currents have the least contribution to the amplitude of Chandler wobble excitation function, approximately 1/6 of the total amplitude excited by the Pacific, Indian and Atlantic currents. The underprediction in our calculated Chandler wobble excitation function is thus expected because, as observations show, the North Atlantic ocean region is not the biggest contributor to the Wobble dynamics.

4 CONCLUSIONS

We presented a two-scale single-layer ocean model which well mimics a high fidelity numerical model in terms of overall dynamical effects on Chandler wobble. We parametrized the oceanic turbulence and introduced a secondary solution whose width provides an extra tuning parameter. We found that the distribution of velocity components throughout the whole domain is responsible for the overall angular momentum of the double gyre; however, the upraised velocities in the jet zone contribute the most to the double-gyre kinetic energy content and its rate of energy transfer to the Chandler wobble. Our simplified ocean model admits a fast spectral solution, provides a reasonable approximation to more complex ocean models, and provides a rapid turn-around tool to study the influence of the North Atlantic double-gyre on the Earth's Chandler wobble. Utilizing this calibrated toy model over a wide range of physically relevant parameters, we have found that the feedback from Chandler wobble onto the North Atlantic double-gyre is insignificant. The amplitude of the wobble excitation function predicted by our model shows that the North Atlantic ocean has a small effect on the wobble dynamics as compared to the overall ocean effect. This finding is in agreement with the existing observational data (Ma *et al.* 2009; Nastula *et al.* 2012, 2014).

Table 2. Coefficients of effective angular momentum functions.

$\sqrt{\psi_1^2 + \psi_2^2}$	Spectral	Numerical 256 × 256	Numerical 512 × 512
Full coupling:	2.07081×10^{-9}	2.03852×10^{-9}	2.06514×10^{-9}
Complete de-coupling:	1.929120×10^{-9}	1.899041×10^{-9}	1.923837×10^{-9}

ACKNOWLEDGEMENTS

Funding from Partnership for Observation of Global Oceans and Scientific Committee for Oceanic Research (POGO-SCOR) is gratefully acknowledged by SEN. The work of SK was supported by Natural Environment Research Council grant (NE/H020837/1). MRA acknowledges the support from the American Bureau of Shipping. The authors are grateful to Pavel Berloff and Igor Shevchenko from Imperial College London for making their quasi-geostrophic double-gyre code radially available. We also express our sincere thanks to an anonymous referee and the referee Steven Dickman for their enlightening comments that helped us to improve the presentation of our results. The use of computing resource on Apocrita computer cluster at Queen Mary University of London is gratefully acknowledged.

REFERENCES

Adhikari, S. & Ivins, E.R., 2016. Climate-driven polar motion: 2003–2015, *Sci. Adv.,* **2**(4), e1501693, doi:10.1126/sciadv.1501693.

Aoyama, Y. & Naito, I., 2001. Atmospheric excitation of the Chandler wobble, 1983–1998, *J. geophys. Res.,* **106**(B5), 8941–8954.

Brzeziński, A., Dobslaw, H., Dill, R. & Thomas, M., 2012. Geophysical excitation of the Chandler wobble revisited, in *Geodesy for Planet Earth,* pp. 499–505, eds Kenyon, S., Pacino, M.C. & Marti, U., Springer.

Brzeziński, A. & Nastula, J., 2002. Oceanic excitation of the Chandler wobble, *Adv. Space Res.,* **30**(2), 195–200.

Brzeziński, A., Nastula, J. & Ponte, R.M., 2002. Oceanic excitation of the Chandler wobble using a 50-year time series of ocean angular momentum, in *Vistas for Geodesy in the New Millennium,* pp. 434–439, eds Ádám, J. & Schwarz, K.-P., Springer.

Chao, B.F., 1985. On the excitation of the earth's polar motion, *Geophys. Res. Lett.,* **12**(8), 526–529.

Colombo, G. & Shapiro, I.I., 1968. Theoretical model for the Chandler wobble, *Nature,* 156–157.

Dahlen, F.A., 1971. The excitation of the Chandler wobble by earthquakes, *Geophys. J. Int.,* **25**(1–3), 157–206.

Dickman, S.R., 1983. The rotation of the ocean-solid earth system, *J. geophys. Res.,* **88**(B8), 6373–6394.

Dickman, S.R., 1985. Comments on 'Normal modes of the coupled earth and ocean system' by John M. Wahr, *J. geophys. Res.,* **90**(B13), 11 553–11 556.

Dickman, S.R., 1993. Dynamic ocean-tide effects on Earth's rotation, *Geophys. J. Int.,* **112,** 448–470.

Dickman, S.R., 2003. Evaluation of 'effective angular momentum function' formulations with respect to core–mantle coupling, *J. geophys. Res.,* **108**(B3), 2150–2157.

Dijkstra, H.A., 2006. Interaction of SST modes in the North Atlantic ocean, *J. Phys. Oceanogr.,* **36**(3), 286–299.

Fang, M. & Hager, B.H., 2012. The Ocean de-excites the Chandler wobble, *Am. Geophys. Union, Fall Meeting 2012,* Abstract G51A-1091.

Fengler, M.J., 2005. A nonlinear Galerkin scheme involving vectorial and tensorial spherical wavelets for solving the incompressible Navier-Stokes equation on the sphere, *Proc. Appl. Math. Mech.,* **5,** 457–458.

Furuya, M., Hamano, Y. & Naito, I., 1996. Quasi-periodic wind signal as a possible excitation of Chandler wobble, *J. geophys. Res.,* **101**(B11), 25 537–25 546.

Gross, R.S., 2000. The excitation of the Chandler wobble, *Geophys. Res. Lett.,* **27**(15), 2329–2332.

Gross, R.S., Fukumori, I. & Menemenlis, D., 2003. Atmospheric and oceanic excitation of the Earth's wobbles during 1980–2000, *J. geophys. Res.,* **108**(B8), 2370–2385.

Holland, W.R., 1978. The role of mesoscale eddies in the general circulation of the ocean-numerical experiments using a wind-driven quasi-geostrophic model, *J. Phys. Oceanogr.,* **8**(3), 363–392.

Il'In, A.A. & Filatov, A.N., 1988. Unique solvability of Navier-Stokes equations on a two-dimensional sphere, *Akademiia Nauk SSSR Doklady,* **301,** 18–22.

Karabasov, S.A., Berloff, P.S. & Goloviznin, V.M., 2009. CABARET in the ocean gyres, *Ocean Model.,* **30**(2), 155–168.

Karabasov, S.A. & Goloviznin, V.M., 2009. Compact Accurately boundary-adjusting high-resolution technique for fluid dynamics, *J. Comput. Phys.,* **228**(19), 7426–7451.

Lewis, G.M. & Langford, W.F., 2008. Hysteresis in a rotating differentially heated spherical shell of Boussinesq fluid, *SIAM J. Appl. Dyn. Sys.,* **7**(4), 1421–1444.

Ma, J., Zhou, Y.H., Liao, D.C. & Chen, J.L., 2009. Excitation of Chandler wobble by Pacific, Indian and Atlantic Oceans from 1980 to 2005, *Chin. Astron. Astrophy.,* **33**(4), 410–420.

Munk, W.H. & MacDonald, G.J.F., 1975. *The Rotation of the Earth: A Geophysical Discussion,* Cambridge Univ. Press.

Nastula, J., Salstein, D.A. & Gross, R.S., 2014. Regional multi-fluid-based geophysical excitation of polar motion, in *Earth on the Edge: Science for a Sustainable Planet,* pp. 467–472, eds Rizos, C. & Willis, P., Springer.

Nastula, J., Gross, R.S. & Salstein, D.A., 2012. Oceanic excitation of polar motion: identification of specific oceanic areas important for polar motion excitation, *J. Geodyn.,* **62,** 16–23.

Smagorinsky, J., 1963. General circulation experiments with the primitive equations: I. The basic experiment, *Mon. Weather Rev.,* **91**(3), 99–164.

Shevchenko, I.V. & Berloff, P.S.2015. Multi-layer quasi-geostrophic ocean dynamics in eddy-resolving regimes, *Ocean Modelling,* **94,** 1–14.

Smith, M.L. & Dahlen, F.A., 1981. The period and Q of the Chandler wobble, *Geophys. J. Int.,* **64**(1), 223–281.

Wahr, J.M., 1982. The effects of the atmosphere and oceans on the Earth's wobble – I. Theory, *Geophys. J. Int.,* **70**(2), 349–372.

Wahr, J.M., 1983. The effects of the atmosphere and oceans on the Earth's wobble and on the seasonal variations in the length of day – II. Results, *Geophys. J. Int.,* **74**(2), 451–487.

Wahr, J.M., 1984. Normal modes of the coupled earth and ocean system, *J. geophys. Res.,* **89,** 7621–7630.

Xu, C., Sun, W. & Chao, B.F., 2014. Formulation of coseismic changes in Earth rotation and low-degree gravity field based on the spherical Earth dislocation theory, *J. geophys. Res.,* **119**(12), 9031–9041.